



Formation of a Matter-Wave Bright Soliton

L. Khaykovich, et al. Science **296**, 1290 (2002); DOI: 10.1126/science.1071021

This copy is for your personal, non-commercial use only.

If you wish to distribute this article to others, you can order high-quality copies for your colleagues, clients, or customers by clicking here.

Permission to republish or repurpose articles or portions of articles can be obtained by following the guidelines here.

The following resources related to this article are available online at www.sciencemag.org (this infomation is current as of March 28, 2011):

Updated information and services, including high-resolution figures, can be found in the online version of this article at:

http://www.sciencemag.org/content/296/5571/1290.full.html

Supporting Online Material can be found at:

http://www.sciencemag.org/content/suppl/2002/05/15/296.5571.1290.DC1.html

This article cites 17 articles, 1 of which can be accessed free: http://www.sciencemag.org/content/296/5571/1290.full.html#ref-list-1

This article has been cited by 573 article(s) on the ISI Web of Science

This article has been **cited by** 2 articles hosted by HighWire Press; see: http://www.sciencemag.org/content/296/5571/1290.full.html#related-urls

This article appears in the following **subject collections**:

http://www.sciencemag.org/cgi/collection/physics

tunnel framed by universally conserved basic amino acids (Fig. 6B). Because open complex formation occurs without breaking covalent bonds in the DNA, the RNAP claws must open at some point during the process of open complex formation to allow the template strand to slip into its channel. Subsequent closure of the claws would then establish the tunnel. This requirement for prior states (intermediates) during the steps of open complex formation with different conformations of the enzyme, combined with the good match between footprinting data and the complete open complex model, leads us to suggest that the complex represented in this holoenzyme/fork-junction structure closely resembles the final RP_o.

The RF structure, and the models derived from it, raise key questions that are central to understanding transcription initiation. How is RP_o generated from RP_c (Fig. 5A)? How do transcription activators interact with the complex to enhance the rate of transcription initiation? The structures and models presented here provide a basis for designing more decisive experiments probing these questions and more.

References and Notes

- K. S. Murakami, S. Masuda, S. A. Darst, Science 296, 1280 (2002).
- 2. P. L. deHaseth, M. L. Zupancic, M. T. J. Record, J. Bacteriol. 180, 3019 (1998).
- 3. Y. Guo, J. D. Gralla, Proc. Natl. Acad. Sci. U.S.A. 95, 11655 (1998).
- 4. T. Gaal et al., Mol. Microbiol. 42, 939 (2001).
- 5. S. Keilty, M. Rosenberg, J. Biol. Chem. 262, 6389
- 6. L. Tsujikawa, O. Tsodikov, P. de Haseth, Proc. Natl. Acad. Sci. U.S.A. 99, 3493 (2002).
- 7. E. A. Campbell et al., Cell 104, 901 (2001).
- 8. G. Zhang et al., Cell 98, 811 (1999).

- 9. E. A. Campbell et al., Mol. Cell 9, 527 (2002).
- 10. In the crystal, two DNA fork junctions pack against each other at their blunt, upstream ends (Fig. 1A), forming a pseudo-continuous double-helix related by a crystallographic twofold symmetry axis perpendicular to the DNA helical axis. Thus, the double-stranded upstream ends of the symmetry-related fork junctions were placed with an end-to-end spacing of 3.4 Å (corresponding to base-pair stacking in doublestranded B-form DNA), with the symmetry axis in the
- 11. M. L. Craig, W.-C. Suh, M. T. J. Record, Biochemistry **34**, 15624 (1995).
- 12. J. Mecsas, D. W. Cowing, C. A. Gross, J. Mol. Biol. 220, 585 (1991).
- W. Metzger, P. Schickor, H. Heumann, EMBO J. 8, 2745 (1989).
- 14. P. Schickor, W. Metzger, W. Wladyslaw, H. Lederer, H. Heumann, EMBO J. 9, 2215 (1990).
- K. A. Barne, J. A. Bown, S. J. W. Busby, S. D. Minchin, EMBO J. 16, 4034 (1997).
- C. A. Gross et al., Cold Spring Harbor Symp. Quant. Biol. 63, 141 (1998).
- 17. S. A. Darst et al., in Nucleic Acids & Molecular Biology, F. Ekstein, D. M. J. Lilley, Eds. (Springer, London, 1997), vol. 11, pp. 27–40. 18. B. A. Young *et al.*, *Cell* **105**, 935 (2001).
- 19. X. Huang, F. J. Lopez de Saro, J. D. Helmann, Nucleic Acids Res. 25, 2603 (1997).
- 20. M. Tomsic et al., J. Biol. Chem. 276, 31891 (2001).
- O. N. Ozoline, M. A. Tsyganov, Nucleic Acids Res. 23, 4533 (1995).
- 22. M. Buckle, I. K. Pemberton, M.-A. Jacquet, H. Buc, J. Mol. Biol. 285, 955 (1999).
- D. W. Cowing, J. Mecsas, M. T. J. Record, C. A. Gross,
- J. Mol. Biol. 210, 521 (1989). 24. R. T. Kovacic, J. Biol. Chem. 262, 13654 (1987).
- 25. R. L. Gourse, W. Ross, T. Gaal, Mol. Microbiol. 37, 687 (2000).
- Y. H. Jeon et al., Science 270, 1495 (1995).
- Y. H. Jeon, T. Yamazaki, T. Otomo, A. Ishihama, Y. Kyogoku, J. Mol. Biol. 267, 953 (1997).
- R. H. Ebright, S. Busby, Curr. Opin. Genet. Devel. 5, 197 (1995).
- W. Ross, A. Ernst, R. L. Gourse, Genes Dev. 15, 491
- E. Nudler, E. Avetissova, V. Markovtsov, A. Goldfarb, Science 273, 211 (1996).

- 31. S. A. Weston, A. Lahm, D. Suck, J. Mol. Biol. 226, 1237 (1992).
- T. M. Gruber, D. A. Bryant, J. Bacteriol. 179, 1734 (1997).
- 33. M. Lonetto, M. Gribskov, C. A. Gross, J. Bacteriol. 174, 3843 (1992)
- 34. Y. Harada et al., Nature 409, 113- (2001).
- 35. T. A. Jones, J.-Y. Zou, S. Cowan, M. Kjeldgaard, Acta Crystallogr. A 47, 110 (1991).
- A. Nicholls, K. A. Sharp, B. Honig, Proteins Struct. Funct. Genet. 11, 281 (1991).
- 37. M. Carson, J. Appl. Crystallogr. 24, 958 (1991).
- R. Lavery, H. Sklenar, J. Biomol. Struct. Dyn. 6, 63
- Z. Otwinowski, in Proceedings of the CCP4 Study Weekend, W. Wolf, P. R. Evans, A. G. W. Leslie, Eds. (SERC Daresbury Laboratory, Warrington, UK, 1991) pp. 80-86.
- 40. N. Casan-Pastor, P. Gomez-Romero, G. B. Jameson, L. C. W. Baker, J. Am. Chem. Soc. 113, 5685 (1991).
- We thank M. Pope for the gift of the W₁₂ cluster, G. Schneider for the gift of Ta₆Br₁₄, and T. Gaal and R. Gourse for providing the full con promoter sequence before publication; D. Thiel and the staff at the Cornell High Energy Synchrotron Source and M. Becker and L. Berman at NSLS X25 for support during data collection; K. Kinosita and R. Landick for important discussion; and D. Jeruzalmi, S. Nair, and H. Yamaguchi for invaluable advice. Figure 1B was made using the program O (35). Figures 2, 4, 5, and 6 were made using the program GRASP (36). Figure 3 was made using the program RIBBONS (37). Supported by a Norman and Rosita Winston Postdoctoral Fellowship and a Human Frontiers Sciences Program Postdoctoral Fellowship (K.S.M.); National Research Service Award number NIH GM20470 (E.A.C.); and, in part, by NIH grants GM53759 and GM61898 (S.A.D.)

Supporting Online Material

(www.sciencemag.org/cgi/content/full/296/5571/ 1285/DC1) Material and Methods

References and notes fig. S1

7 January 2002; accepted 21 March 2002

Formation of a Matter-Wave **Bright Soliton**

L. Khaykovich, ¹ F. Schreck, ¹ G. Ferrari, ^{1,2} T. Bourdel, ¹ J. Cubizolles, L. D. Carr, Y. Castin, C. Salomon 1*

We report the production of matter-wave solitons in an ultracold lithium-7 gas. The effective interaction between atoms in a Bose-Einstein condensate is tuned with a Feshbach resonance from repulsive to attractive before release in a one-dimensional optical waveguide. Propagation of the soliton without dispersion over a macroscopic distance of 1.1 millimeter is observed. A simple theoretical model explains the stability region of the soliton. These matterwave solitons open possibilities for future applications in coherent atom optics, atom interferometry, and atom transport.

Solitons are localized waves that travel over long distances with neither attenuation nor change of shape, as their dispersion is compensated by nonlinear effects. Soliton research has been conducted in fields as diverse as particle physics, molecular biology, geology, oceanography, astrophysics, and nonlin-

ear optics. Perhaps the most prominent application of solitons is in high-rate telecommunications with optical fibers (1).

We use a Bose-Einstein condensate (BEC) of a dilute atomic gas of lithium atoms as a macroscopic matter-wave to form a soliton. Nonlinearity is provided by binary atomic in-

teractions leading to the mean-field potential $U(\vec{r}) = gn(\vec{r}) = 4\pi\hbar^2 an(\vec{r})/m$, where a is the scattering length, $n(\vec{r})$ the spatial density, and m the atomic mass. For a < 0 the effective interaction is attractive, and a trapped BEC is only stable for a number of atoms less than a critical number above which collapse occurs (2-4). When the BEC is confined in only two directions, matter-waves have dispersion in the free direction owing to their kinetic energy, $E_{\rm kin} \propto k^2$, where k is the atomic wave vector. The balance between this dispersion and the attractive mean-field energy can lead to the formation of bright solitons as shown theoretically (5-7). Until now, only dark solitons have been observed in BECs with repulsive interactions (a > 0)

¹Laboratoire Kastler Brossel, Ecole Normale Supérieure, 24 rue Lhomond, 75231 Paris Cedex 05, France. ²European Laboratory for Non-Linear Spectroscopy-Istituto Nazíonale per la Fisica della Materia, Largo E. Fermi 2, Firenze 50125, Italy

^{*}To whom correspondence should be addressed. Email: salomon@lkb.ens.fr

(8, 9). These solitons are characterized by a notch in the BEC density profile with a phase step across the soliton center. They propagate within the BEC with a velocity less than the speed of sound, but so far are found to decay before reaching the edge of the condensate.

We report the formation of a matter-wave bright soliton, a freely propagating self-bound atomic gas. The soliton is produced from a $^7\mathrm{Li}$ BEC in the internal atomic state $|F=1,\,m_F=1\rangle.$ In this state a Feshbach resonance allows us to continuously tune the scattering length from a positive to negative value by means of an applied magnetic field (10, 11), a requirement for the production of a bright soliton.

In our experimental setup (12–14), 4 \times 10⁸ 7 Li atoms are loaded from a magneto-optical trap into a strongly confining Ioffe-Pritchard (IP) magnetic trap. Atoms are in the $|F=2,m_F=2\rangle$ state for which the scattering length is a=-1.4 nm. Evaporative cooling lowers the temperature from 2 mK to 10 μ K, after which \sim 6 \times 10⁵ atoms remain. Atoms are then transferred into a far detuned optical dipole trap at the intersection of two Nd:YAG (yttrium-aluminum-garnet) Gaussian laser beams (Fig. 1) with common waists of 38(3) μ m (15). The 9.5, W laser power is split between the two beams by means of two acousto-optic modulators.

The transfer from the magnetic trap to the optical trap is done in two steps. First, the power of the YAG beams is ramped over 200 ms to a value such that the radial oscillation frequency of the atoms is 1.8 kHz in the vertical beam and 3.3 kHz in the horizontal beam, which matches that of the IP trap. Second, the magnetic trap is slowly turned off over 200 ms,

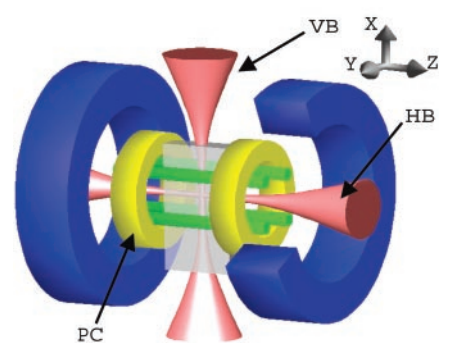


Fig. 1. Experimental setup for soliton production. ^7Li atoms are evaporatively cooled in a loffe-Pritchard magnetic trap and transferred into a crossed optical dipole trap in state $|F=1,m_F=1\rangle$ where they Bose condense. Magnetic tuning of the scattering length to positive, zero, and negative values is performed with the two pinch coils (PC). Switching-off the vertical trapping beam (VB) allows propagation of a soliton in the horizontal 1D waveguide (HB). Absorption images of solitons and BECs are recorded on a charge-coupled device camera in the x, z plane.

keeping only a 5-G bias field. The transfer efficiency is nearly 100%. Then, transfer from the state $|F=2, m_F=2\rangle$ to the state |F=1, $m_F = 1$ is performed by rapid adiabatic passage with a microwave-frequency sweep scanning 1 MHz in 10 ms at ~820 MHz. The transfer efficiency is better than 95%. Among all 7 Li hyperfine states that can be trapped in the dipole trap, $|F = 1, m_F = 1\rangle$ is particularly useful as it is the lowest energy state in which two-body losses, which are relatively strong in the state $|F = 2, m_F = 2\rangle$ (13), are completely suppressed. Furthermore, this state is predicted to have a Feshbach resonance near 725 G (11), allowing magnetic tuning of the scattering length (Fig. 2). An adjustable magnetic field is produced by the pinch coils of our IP trap. Their inductance is small so that their current can be changed on a time scale shorter than \sim 200 μ s. As in previous work on ²³Na and ⁸⁵Rb (16, 17), we locate the 7Li Feshbach resonance through observation of a dramatic loss of trapped atoms that we experimentally identify as being due to three-body recombination. The resonance position is found at 720(15) G, in good agreement with theory (725 G) (11).

We then produce a ⁷Li BEC in the crossed dipole trap by forced evaporation achieved by lowering the depth of the optical trapping potential (18). Between B = 0 and B = 590 G, the scattering length is small ($|a| \le 0.4$ nm), hindering efficient evaporative cooling (Fig. 2). Therefore, we operate at a magnetic field of 665 G in the wing of the Feshbach resonance where $a \cong +2.1$ nm and where three-body losses remain moderate. The horizontal (vertical) optical power is lowered from 5.5 W (1.5 W) to 1.15 W (0.9 W) in 100 ms, and then to 0.27 W (0.19 W) in 150 ms. A condensate with $N \sim$ 2×10^4 atoms, about half of the total number of atoms, is obtained in a nearly isotropic trap where atoms have oscillation frequencies of 710, 1000, and 710 Hz along *x*, *y*, and *z* axes. We then tune the scattering length to zero to reduce three-body losses.

To transform the BEC into a bright soliton, the trapping geometry is adiabatically deformed to a cylindrical geometry obtained by keeping only the horizontal trapping beam. To ensure adiabatic deformation of the condensate, the vertical beam power is ramped down to 3 mW in 200 ms, which reduces the axial oscillation frequency of the atoms to $\omega_z \cong 2\pi \times 50~\text{Hz}$ while the radial oscillation frequency remains $\omega_{\perp}=2\pi\times710$ Hz. The effective interaction is then tuned through changes in the magnetic field in 50 ms. Finally, switching off the vertical beam with a mechanical shutter releases the BEC into the horizontal one-dimensional (1D) waveguide. In the axial direction, the coils that are used to provide the offset field produce a slightly expulsive harmonic potential for the state $|F = 1, m_F = 1\rangle$, which overcomes the dipole trap. The resulting axial force on the atoms is conveniently written as $-m\omega_z^2 z$, where the frequency ω_z is now imaginary. Typically, $\omega_z = 2i\pi \times 78$ Hz for B = 520 G. After an adjustable evolution time in the horizontal guide, the bias magnetic field is turned off, and 400 µs later an absorption image is recorded (Fig. 3; see supplemental movie on Science Online at www.sciencemag.org/cgi/content/ full/296/5571/1290/DC1) where the formation of the soliton is seen.

We compare the evolution of an ideal gas (Fig. 3A), $a \approx 0$ for B = 520 G, with a gas with attractive interactions (Fig. 3B), a = -0.21 nm for B = 425 G. In both cases the cloud drifts toward the left because of a small offset, ≈50 µm, between the maximum of the expulsive potential and the initial position of the atoms. The width of the expanding cloud in the horizontal waveguide is considerably broader in the noninteracting case, while for all times of observation the soliton width remains equal to the resolution limit of our imaging system, 9(1) µm axially (19). The cloud contains $6(2) \times 10^3$ atoms and propagates over a distance of 1.1 mm without any detectable dispersion, a clear signature of a bright soliton (20). No decay of the soliton is observed in the 10 ms it remains in the detection region. A substantial fraction of

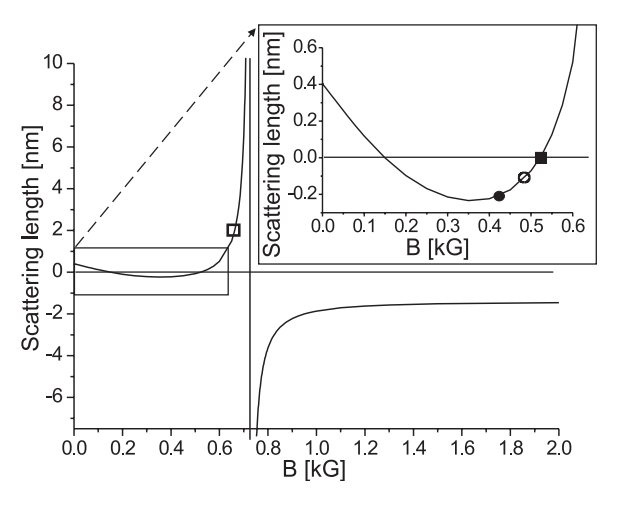


Fig. 2. Predicted magnetic field dependence of the scattering length a for ^7Li in state |F=1, $m_F=1\rangle$ (11). (Inset) Expanded view of the 0 to 0.6 kG interval with the various values of a used to study soliton formation. (□) Initial BEC; (■) ideal BEC gas; (○) attractive gas; (●) soliton.

atoms, $\approx 2/3$, remains in a noncondensed pedestal around the soliton, clearly visible for intermediate propagation times in the guide.

We then made measurements of the wavepacket size versus propagation time for three values of the scattering length: $a \approx 0$, $a \approx$ -0.11 nm, and $a \approx -0.21$ nm (Fig. 4). For a ≈ 0 (Fig. 4A), the interaction between atoms is negligible, and the size of the cloud is governed by the expansion of the initial condensate distribution under the influence of the negative curvature of the axial potential. The measured size is in excellent agreement with the predicted size of a noninteracting gas subjected to an expulsive harmonic potential: Taking the curvature as a fit parameter (solid line in Fig. 4A), we find $\omega_z = 2i\pi \times 78(3)$ Hz, which agrees with the expected value of the curvature produced by the pinch coils (14). For a = -0.11 nm and B = 487 G, the size of the wave packet is consistently below that of a noninteracting gas (Fig. 4B, solid line). Attractive interactions reduce the size of the atomic cloud but are not strong enough to stabilize the soliton against the expulsive potential. When a is further decreased to -0.21 nm, the measured size of the wave packet no longer changes as a function of guiding time, indicating propagation without dispersion even in the presence of the expulsive potential (Fig. 4C).

Fig. 3. Absorption images at variable delays after switching off the vertical trapping beam. Propagation of an ideal BEC gas (A) and of a soliton (B) in the horizontal 1D waveguide in the presence of an expulsive potential. Propagation without dispersion over 1.1 mm is a clear signature of a soliton. Corresponding axial profiles are integrated over the vertical direction.

Fig. 4. Measured root mean square size of the atomic wave packet Gaussian fit as a function of propagation time in the waveguide. (A)
$$a=0$$
, ideal gas case; (B) $a=-0.11$ nm; (C) $a=-0.21$ nm; solid lines: calculated expansion of a noninteracting gas in the expulsive potential.

To theoretically analyze the stability of the soliton, we introduce the 3D Gross-Pitaevskii energy functional

$$\begin{split} E_{\rm GP} &= \int d^3r \, \frac{\hbar^2}{2m} \big| \nabla \Psi(\vec{r}) \big|^2 + \frac{Ng}{2} \big| \Psi(\vec{r}) \big|^4 \\ &+ \frac{1}{2} \, m \, \big[\omega_\perp^2(x^2 + y^2) + \omega_z^2 z^2 \big] \big| \Psi(\vec{r}) \big|^2 \end{split}$$

where the condensate wave function Ψ is normalized to 1. In Eq. 1 the first term is the kinetic energy responsible for dispersion; the second term is the interaction energy, which in the present case of attractive effective interactions (g < 0) causes the wave function to sharpen; and the third term is the external potential energy. We introduce the following two-parameter variational ansatz to estimate minimal-energy states of $E_{\rm GP}$:

$$\Psi(\vec{r}) = \frac{1}{\sqrt{2\pi\sigma_{\perp}^{2}l_{z}}} \frac{1}{\cosh(z/l_{z})} \exp\left(-\frac{x^{2} + y^{2}}{2\sigma_{\perp}^{2}}\right)$$
(2)

where σ_{\perp} and l_z are the radial and axial widths of the wave function. The functional form of the well-known 1D soliton has been chosen for the longitudinal direction (5), while in the transverse direction a Gaussian ansatz is the optimal one for harmonic con-

finement. For each l_z we minimize the mean energy over σ_{\perp} ; the resulting function of l_z is plotted (Fig. 5) for various values of the parameter Na/a_{\perp}^{ho} where $a_{\perp}^{\text{ho}} = (\hbar/m\omega_{\perp})^{1/2}$. For very small axial sizes, the interaction energy becomes on the order of $-\hbar \omega_{\perp}$ and the gas loses its quasi-1D nature and collapses (3, 4). For very large axial sizes, the expulsive potential energy dominates and pulls the wave function apart. For intermediate sizes, attractive interactions balance both the dispersion and the effect of the expulsive potential; the energy presents a local minimum (solid line in Fig. 5). This minimum supports a macroscopic quantum bound state. However, it exists only within a narrow window of the parameter Na/a_{\perp}^{ho} . In our experiments $\omega_{\perp} = 2\pi \times 710 \text{ Hz}$ and $\omega_{z} = 2i\pi \times 710 \text{ Hz}$ 70 Hz for B = 420 G, so that $a_{\perp}^{\text{ho}} = 1.4 \text{ }\mu\text{m};$ for N|a| larger than $(N|a|)_c = 1.105 \mu m$, a

For our experimental conditions and a=-0.21 nm, the number of atoms that allows the soliton to be formed is $4.2\times 10^3 \le N \le 5.2\times 10^3$, in good agreement with our measured number $6(2)\times 10^3$. The expected axial size of the soliton is $l_z\cong 1.7$ µm, which is below the current resolution limit of our imaging system. To verify the presence of a critical value of $N|a|_e$ needed to stabilize the soliton, we have performed the measurements with the same a but with a reduced number of atoms, $N=2\times 10^3$. At 8 ms guiding time the axial size of the wave packet increased to 30 µm, indicating that no soliton was formed.

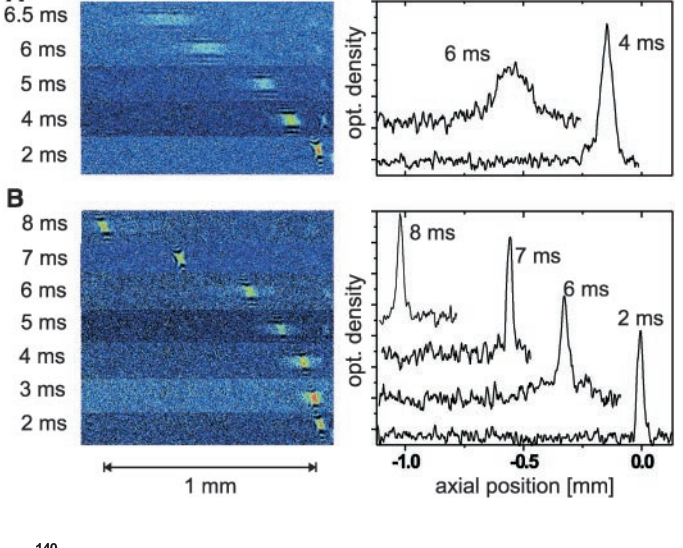
collapse occurs (dashed curve in Fig. 5),

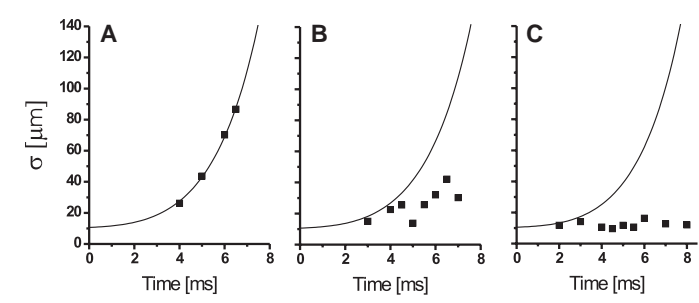
while for N|a| smaller than $(N|a|)_e = 0.88$

µm the expulsive potential causes the gas to

explode axially (dotted curve in Fig. 5).

One may speculate as to the formation dynamics of the soliton in the elongated trap before its release in the optical waveguide. Because the atom number in the initial BEC, $2 \times$





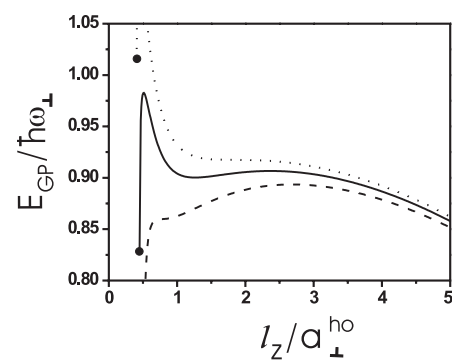


Fig. 5. Theoretical energy diagram of an attractive Bose gas subjected to an expulsive potential for $\omega_z/\omega_\perp=i\times70/710$. The energy as a function of the axial size after minimization over the tranverse size is shown for three values of N|a|: within the stability window (solid curve), at the critical point for explosion $(N|a|)_e$ (dotted curve), and at the critical point for collapse $(N|a|)_c$ (dashed curve). End points of the curves indicate collapse, i.e., $\sigma_1=0$.

104, is about three times as large as the measured atom number in the soliton, it is likely that during the 50 ms phase where a is changed from 0 to negative values, one or several collapses occur until the critical number for a stable BEC is reached. Indeed, the collapse time constant is predicted to be much less than 50 ms for our experimental conditions (21). During the transfer into the 1D waveguide, the BEC is transformed into a soliton and the noncondensed cloud is clearly observed at guiding times up to 6 ms as a broader background distribution. Nonadiabatic projection of the BEC from the confining onto the expulsive potential is expected to play a negligible role here, according to numerical simulations (22). At longer times, the noncondensed atoms spread apart and become undetectable. Thus, during the propagation phase the soliton decouples itself from the noncondensed fraction, resulting in a nearly pure soliton.

Finally, removal of the expulsive axial potential will allow us to extend the stability domain toward lower values of N|a| and

longer observation times. The soliton size could then be measured in situ, as well as its lifetime. The study of coherence properties of solitons and of binary collisions between solitons is an immediate extension of the present work

References and Notes

- See, for example, the recent special issue: Chaos 10, 471 (2000).
- P. A. Ruprecht, M. J. Holland, K. Burnett, M. Edwards, *Phys. Rev. A* 51, 4704 (1995).
- C. C. Bradley, C. A. Sackett, R. G. Hulet, *Phys. Rev. Lett.* 78, 985 (1997).
- 4. J. L. Roberts *et al.*, *Phys. Rev. Lett.* **86**, 4211 (2001).
- V. E. Zakharov, A. B. Shabat, Sov. Phys. JETP 34, 62 (1972).
- V. M. Pèrez-Garcìa, H. Michinel, H. Herrero, *Phys. Rev.* A 57, 3837 (1998).
- J. Sos (1996).
 L. D. Carr, M. A. Leung, W. P. Reinhardt, J. Phys. B 33, 3983 (2000).
- 8. S. Burger et al., Phys. Rev. Lett. 83, 5198 (1999).
- 9. J. Denschlag et al., Science 287, 97 (2000).
- E. Tiesinga, B. J. Verhaar, H. T. S. Stoof, *Phys. Rev. A* 47, 4114 (1993).
- 11. V. Venturi, C. Williams, personal communication.
- M.-O. Mewes, G. Ferrari, F. Schreck, A. Sinatra, C. Salomon, *Phys. Rev. A* 61, 011403R (2000).
- 13. F. Schreck et al., Phys. Rev. A 64, 011402R (2001).

- 14. F. Schreck et al., Phys. Rev. Lett. 87, 080403 (2001).
- See, for instance, R. Grimm, M. Weidemüller, Y. B. Ovchinnikov, Adv. At. Mol. Opt. Phys. 42, 95 (2000).
- 16. S. Inouye et al., Nature 392, 151 (1998).
- J. L. Roberts, N. R. Claussen, S. L. Cornish, C. E. Wieman, *Phys. Rev. Lett.* 85, 728 (2000).
- M. D. Barrett, J. A. Sauer, M. S. Chapman, *Phys. Rev. Lett.* 87, 010404 (2001).
- In the vertical direction, a residual astigmatism of the imaging system gives a resolution limit of 16 μm.
- 20. Over this distance, the change in magnetic field due to the curvature is 0.1 G, and therefore the change in the scattering length is negligible (Fig. 2).
- Y. Kagan, A. E. Muryshev, G. V. Shlyapnikov, *Phys. Rev. Lett.* 81, 933 (1998).
- 22. L. D. Carr. Y. Castin. in preparation.
- 23. We are grateful to K. Corwin, M. Olshanii, G. Shlyapnikov, C. Williams, V. Venturi, and B. Esry for important contributions to this work and to J. Dalibard and C. Cohen-Tannoudji for useful discussions. Supported by the DAAD (F.S.), the European Union network CT 2000-00165 CAUAC (G.F.), and the NSF MPS-DRF 0104447 (L.D.C.). This work was supported by CNRS, Collège de France and Région Ile de France. Laboratoire Kastler Brossel is Unité de recherche de l'Ecole Normale Supérieure et de l'Université Pierre et Marie Curie, associated with CNPS.

19 February 2002; accepted 5 April 2002

Semiconductor NCs have been prepared

Electrochemistry and Electrogenerated Chemiluminescence from Silicon Nanocrystal Quantum Dots Zhifeng Ding. Bernadette M. Quinn. Santosh K. Haram. 1

Zhifeng Ding, Bernadette M. Quinn, Santosh K. Haram, Lindsay E. Pell, Brian A. Korgel, Allen J. Bard*

Reversible electrochemical injection of discrete numbers of electrons into sterically stabilized silicon nanocrystals (NCs) (~2 to 4 nanometers in diameter) was observed by differential pulse voltammetry (DPV) in N,N'-dimethylformamide and acetonitrile. The electrochemical gap between the onset of electron injection and hole injection—related to the highest occupied and lowest unoccupied molecular orbitals—grew with decreasing nanocrystal size, and the DPV peak potentials above the onset for electron injection roughly correspond to expected Coulomb blockade or quantized double-layer charging energies. Electron transfer reactions between positively and negatively charged nanocrystals (or between charged nanocrystals and molecular redox-active coreactants) occurred that led to electron and hole annihilation, producing visible light. The electrogenerated chemiluminescence spectra exhibited a peak maximum at 640 nanometers, a significant red shift from the photoluminescence maximum (420 nanometers) of the same silicon NC solution. These results demonstrate that the chemical stability of silicon NCs could enable their use as redox-active macromolecular species with the combined optical and charging properties of semiconductor quantum dots.

In a bulk semiconductor, electrons and holes move freely throughout the crystal. However, in a nanocrystal, confinement of the electrons and holes leads to a variety of optical and electronic consequences, including size-dependent molecular-like optical properties, greater electron/hole overlap for enhanced photoluminescence (PL) efficiencies, and discrete single-electron/hole charging. Because of their

enormous surface area—to—volume ratios, nanocrystals (NCs) are highly susceptible to heterogeneous redox chemistry with the surrounding environment. Depending on the semiconductor and the surface chemistry, this chemical reactivity can lead to either fatal chemical degradation or new useful properties, such as reversible photocatalytic and electrochromic properties and redox reactivity.

with narrow size distributions, controlled surface chemistry, and internal bulk crystal structure (1, 2), and adsorbed capping ligands are often used to control size and prevent irreversible aggregation. Although the electrochemical properties of monolayer-protected metallic NCs have been well documented (3, 4), reports concerning the electrochemical properties of semiconductor NCs remain scarce (5–9). Difficulties include the limited potential window available in aqueous solutions, the limited solubility of many NCs in nonaqueous solvents, and the need for highly pure, isolated, monodisperse dots. Compound semiconductor NCs, such as CdS, are also chemically unstable upon electron transfer. For example, CdS NCs are irreversibly oxidized and reduced when electron transfer occurs at an electrode (9). Elemental semiconductor NCs, such as Si and Ge, should be more stable. Here we show that monolayer-protected Si NCs are chemically stable upon electron and hole injection; furthermore, electron/hole annihilation through electron transfer reactions between NCs, or NCs with redox-active coreactants, leads to visible light production [electrogenerated chemiluminescence (ECL)].

We recently developed a new synthetic strategy to produce Si NCs terminated with a

1293

¹Department of Chemistry and Biochemistry, ²Department of Chemical Engineering, Center for Nanoand Molecular Science and Technology, Texas Materials Institute, The University of Texas at Austin, Austin, TX 78712, USA.

^{*}To whom correspondence should be addressed. E-mail: ajbard@mail.utexas.edu (A.J.B.); korgel@mail.che.utexas.edu (B.A.K.).